



# Sea level variability in the Gulf of Mexico since 1900 and its link to the Yucatan Channel and the Florida Strait flows

Tal Ezer<sup>1</sup>

Received: 2 June 2022 / Accepted: 18 October 2022 / Published online: 27 October 2022  
© Springer-Verlag GmbH Germany, part of Springer Nature 2022

## Abstract

The long-term variability of sea level and surface flows in the Gulf of Mexico (GOM) is studied using global monthly sea level reconstruction (RecSL) for 1900–2015. The study explored the long-term relation between the dynamics of the GOM and inflows/outflows through the Yucatan Channel (YC) and the Florida Straits (FS). The results show a century-long trend of increased mean velocity and variability in the Loop Current (LC); however, no significant upward trend was found in the YC and FS flows, only increased variability. Empirical orthogonal function (EOF) analysis of sea surface height found spatial patterns dominated by variations in the LC and temporal variations on time scales ranging from a few months to multidecadal. The time evolution of each EOF mode of sea level is correlated with the velocity of either the LC, the YC, or the FS or some combination of the different flows. The mean sea level difference between the GOM and the northwestern Caribbean Sea was found to be influenced by the North Atlantic Oscillation (NAO), with unusually high differences during the 1970s when the NAO index was low and the Atlantic Ocean circulation was weak. Extreme peaks in SL difference coincide with the extension of the LC and the seasonal eddy shedding pattern. The observed seasonal cycle in the extension area of the LC as obtained from 20 years of altimeter data is significantly correlated ( $R=0.63$ ; confidence level = 98%) with the seasonal YC flow obtained from 116 years of the RecSL data. However, the same LC extension record had lower correlation ( $R=0.45$ ; confidence level = 90%) with the observed YC transport obtained from direct moored measurements over ~5 years, indicating the need for much longer measurements, since the LC extension and the YC flow are strongly affected by interannual and decadal variations. The study demonstrates the usefulness of even a coarse-resolution reconstruction for studies of regional ocean variability and climate change over longer time scales than current direct observations allow.

**Keywords** Gulf of Mexico · Loop Current · Sea level · Climate change

## 1 Introduction

The Gulf of Mexico (GOM) is a semi-enclosed basin with complex geography and interesting ocean dynamics (Fig. 1). The dynamics is dominated by variations in the warm Loop Current (LC) which periodically shed westward propagating eddies at different intervals (Sturges and Leben 2000). The region plays an important role in the circulation of the Atlantic Ocean, since the western boundary current (WBC) must pass through the GOM, starting from the Caribbean

Current that enters the GOM from the Yucatan Channel (YC) to feed the LC and then exiting the GOM through the Florida Strait (FS) to form the Florida Current (FC), which evolved downstream into the Gulf Stream. The GOM is an important source of oil and gas drilling, so its coasts can be affected by oil spills (e.g., Beyer et al. 2016) as well as by sea level rise (e.g., Kolker et al. 2011) and tropical storms and hurricanes (Oey et al. 2006; Prasad and Hogan 2007; Chen et al. 2008). Understanding the ocean dynamics in the GOM may be important for addressing all these issues.

In the early days, the GOM has been studied mostly with limited observations that include hydrographic surveys, current meter data, and early infrared satellite images (Reid 1972; Maul 1977; Molinari et al. 1978; Vukovich et al. 1979; Elliott 1982; Sturges and Evans 1983; Maul et al. 1985) and later with XBT and ARGOS data (Hamilton et al. 2002), following with satellite altimeter data (Hamilton et al. 2014; Nickerson

---

Responsible Editor: Andrea Pinones

✉ Tal Ezer  
tezer@odu.edu

<sup>1</sup> Center for Coastal Physical Oceanography, Old Dominion University, 4111 Monarch Way, Norfolk, VA 23508, USA

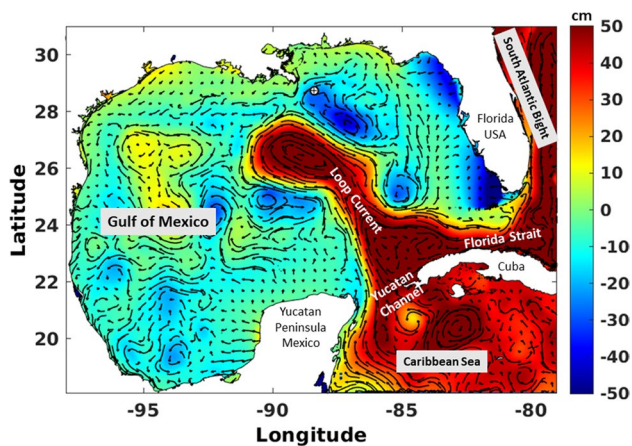


**Fig. 1** Example of daily sea surface height (in cm) and velocity in the Gulf of Mexico (HYCOM model forecast from the Navy Research Laboratory; <https://www7320.nrlssc.navy.mil/hycomGOM2/>). Geographic locations and ocean features discussed in the text are labeled

et al. 2022). Early numerical models of the GOM were relatively simple with only few layers (Hurlburt and Thompson 1980) and coarse resolution (Blumberg and Mellor 1985) or include only the continental shelf (Hsueh et al. 1982). Later, numerical models evolved into realistic high-resolution ocean circulation models of the entire GOM that can resolve the details of the LC and eddy shedding (Candela et al. 2003; Ezer et al. 2003; Kantha et al. 2005; Oey et al. 2003, 2004, 2005; Prasad and Hogan 2007; Xu et al. 2013; Kourafalou et al. 2017). However, if one wants to study decadal to multi-decadal dynamic variability in the region, most observations, except tide gauges (which are limited to the coast), are too short, with the longest continuous flow observation being the Florida Current transport measurements that started in the early 1980s (Baringer and Larsen 2001; Meinen et al. 2010). Most altimeter data, which can monitor the LC, started in the early 1990s (Ducet et al. 2000), and measurements of the flow in the entire Yucatan Channel started only in 1996 (Bunge et al. 2002; Sheinbaum et al. 2002; Candela et al. 2003).

This lack of long-term data motivated this study which used monthly global reconstructed sea level (RecSL) for 1900–2015; this data set is based on the composition of spatial patterns in altimeter data and temporal variability and trends from tide gauge data (see Dangendorf et al. 2019 and more details in the next section). Since this data set has relatively coarse resolution ( $1^\circ \times 1^\circ$ ), it is not expected to resolve mesoscale features such as the details of the LC as models and other data do (e.g., Hamilton et al. 2014; Nickerson et al. 2022). However, one of the goals of the study was to test if the global RecSL can be used in regional studies to detect long-term variability and change in ocean dynamics and interaction between open ocean dynamics and coastal sea level (Dangendorf et al. 2021; Ezer and Dangendorf 2020, 2021, 2022). Analyzing a century-long record is especially

important in the GOM because processes such as LC eddy shedding events are unpredictable and infrequent. Sturges and Leben (2000), for example, detected 34 eddy separation events between 1973 and 1999 with typical separation periods of 6–11 months. Using SST, chlorophyll, and hydrostatic data, Hamilton et al. (2014) reported on 20 eddy separation events between 1978 and 1992 with average separation period of 170 days (but period varied widely from ~80 to 600 days). During the satellite altimeter era, the same report counted 30 eddy separation events between 1992 and 2012, with mean separation period of ~240 days. However, different data and different methods often result in discrepancy in the timing of eddy separation. Many other studies tried to understand different aspects of the dynamics of the LC and eddy separation using different data and different models (Forristal et al. 1992; Bunge et al. 2002; Ezer et al. 2003; Oey et al. 2003, 2005; Oey 2004; Lin et al. 2010; Chang and Oey 2012; Hamilton et al. 2014; Hall and Leben 2016; Nickerson et al. 2022). Several of the above studies linked variations in the LC to variations in the YC flow. Since the YC flow feeds the LC, increased YC flow is expected to cause either expanding of the LC area or increased in the outflow through the FS (or both). Indeed, direct observations of the YC and the FS over 4 years show correlation of 0.83 between the two currents for periods longer than a week (Candela et al. 2019). However, other factors such as winds over the Caribbean Sea (Oey et al. 2003; Athié et al. 2020), the vorticity flux across the YC (Oey 2004), stratification (Moreles et al. 2021), Cuban anticyclones (Kourafalou et al. 2017), or even hurricanes (Oey et al. 2006) can also affect the dynamics of the LC, making connections between forcing and dynamics more complicated. One notes that none of the many GOM studies above could detect multidecadal variability when most data cover periods of only few years to few decades, and the direct observations of the YC flow started in 1996 and are relatively short (Sheinbaum et al. 2002; Bunge et al. 2002; Candela et al. 2003; Athié et al. 2020). One may ask if links between the YC flow, the FS flow, and the LC dynamics exist for periods longer than the interannual time scales of previous studies. Athié et al. (2020), for example, study the seasonal pattern of the YC transport using ~5 years of direct mooring measurements and 23 years of altimeter data; both data show maximum transport in summer (July to August) but disagreed about the month of minimum flow (March in direct observations but November in altimeter data). For a review of the different attempts to describe the seasonal pattern of the LC and eddy shedding and the often discrepancy between different studies, see also Hall and Leben (2016). In any case, the analysis of the long record here can allow to study seasonal patterns over many more years (116) than any past observations and potential connections between the GOM and basin-scale, long-term Atlantic Ocean variability.

The paper is organized as follows: the data and the analysis methods are described in Sect. 2, and then in Sects. 3, the results are described, first for sea level variability and then for potential connections between strait flow and sea level, including potential seasonal and longer trends. Finally, in Sect. 4, summary and conclusions are offered.

## 2 Data sources and analysis methods

The main data source used here to study long-term variability is the monthly global reconstructed sea level (RecSL) data set on a ( $1^\circ \times 1^\circ$ ) grid for 1900–2015 that was developed and described by Dangendorf et al. (2019). This data set was recently used in several studies (Dangendorf et al. 2021; Ezer and Dangendorf 2020, 2021, 2022; Frederikse et al. 2020; Gehrels et al. 2020); these studies demonstrated the usefulness of this data set to better understand not only long-term sea level rise, but also variations in ocean dynamics and connections between the open ocean and the coast. Geostrophic surface velocity obtained from this data was used, for example, to detect past and recent weakening in the Gulf Stream (Ezer and Dangendorf 2020) and a global increase in surface kinetic energy, especially near western boundary currents (Ezer and Dangendorf 2021). This reconstruction is based on the combination of time evolution of long tide gauge records with spatial patterns in satellite altimeter data; it includes sea level rise trends but excludes the seasonal cycle of sea level; for more details of RecSL, see Dangendorf et al. (2019). The main advantage of the RecSL is that it is global and has a long record length (116 years), but the main shortcoming is the coarse resolution ( $1^\circ \times 1^\circ$ ). Since the RecSL is a coarse-resolution data set, direct altimeter data is also used here to look at the LC in more details, using the gridded AVISO (<http://las.avisio.oceanobs.com/>) data set that combined several altimeters (Ducet et al. 2000); the altimeter data are also available from the Copernicus Marine service (<https://marine.copernicus.eu/>).

To represent basin-wide climate variability, the North Atlantic Oscillation Index (NAO) (Hurrell 1995; Hurrell et al. 2003) was obtained from UCAR (<https://climatedataguide.ucar.edu/climate-data/hurrell-north-atlantic-oscillation-nao-index-pc-based>). Many studies show that the NAO is linked with sea level and ocean currents, from the Mediterranean Sea (Tsimplis et al. 2013) to the Gulf Stream (Taylor and Stephens 1998) and to the entire Atlantic Ocean (Ezer and Dangendorf 2022). However, not much research has been conducted so far on the potential impact of NAO on the GOM, except studies related to the impact of NAO on the track of tropical cyclones and landfalls in the GOM region (McCloskey et al. 2013).

From the RecSL data, six monthly time series data sets were extracted and analyzed, 3 for regional mean sea level

and 3 for surface velocity. Time series of mean sea surface height includes 3 subregions (Fig. 1), the Gulf of Mexico (GOMssh), the northwestern Caribbean Sea (CARssh), and the southwestern South Atlantic Bight (SABssh). Time series of surface velocity includes 3 locations, the northward flow in the Yucatan Channel (YCvel) across  $23^\circ\text{N}$ , the eastward flow in the Florida Strait (FSvel) across  $81^\circ\text{W}$ , and the mean velocity speed over the Loop Current (LCvel) in the area  $24^\circ\text{N}$ – $28^\circ\text{N}$  and  $83^\circ\text{W}$ – $87^\circ\text{W}$ . Note, however, that surface velocities obtained from sea surface height slope represent the barotropic flow, but it cannot capture baroclinic velocities and deep counter currents as those observed, for example, in the Yucatan Channel (Bunge et al. 2002; Sheinbaum et al. 2002; Candela et al. 2003).

To analyze spatiotemporal variability in the data, empirical orthogonal function (EOF) analysis is used (also known as principal component analysis (PCA)). A MATLAB code based on early atmospheric and climate data analysis (Bretherton et al. 1992) was used. Oceanographic applications of EOF in the region of interest include studies of the Yucatan Channel flow in observations and models (Candela et al. 2003; Ezer et al. 2003; Oey et al. 2004). The analysis separates data such as sea surface height  $\eta$  into spatial patterns (EOFs) and principal components (PCs) that show how the amplitude of each EOF mode varies in time:

$$\eta(x, y, t) = \sum_{i=1}^n PC_i(t) \cdot EOF_i(x, y) \tag{1}$$

The analysis also calculates the percentage of variability represented by each EOF mode.

To understand what drives each EOF mode, the time series of the first five PCs are compared with time series of strait velocities using empirical mode decomposition (the EMD analysis as developed and described by Huang et al. (1998) and Wu and Huang (2009)). This comparison can detect at which time scales time series are linked or not. EMD decomposes a time series record into  $m$  number of intrinsic mode functions (IMs), each with time-dependent amplitude and frequency, and a long-term residual ( $r$ ). So, for example, a comparison of two velocity time series,  $V1$  and  $V2$ , would yield

$$V1(t) = \sum_{j=1}^m IM1_j(t) + r1(t) ; V2(t) = \sum_{j=1}^m IM2_j(t) + r2(t) \tag{2}$$

$$R_j = COR(IM1_j, IM2_j) ; j = 1, 2, \dots, m$$

$R_j$  is the correlation coefficient between the two velocities for each mode  $j$  (representing different frequency bands). Moreover, PC modes of sea level in (1) can be compared with EMD modes of velocity in (2), providing information, for example, on how variability in strait

velocity is linked with spatiotemporal sea level patterns. Note that due to the filtering effect of EMD, lower frequency modes have reduced the number of degrees of freedom compared with high-frequency modes, so that to achieve the same level of confidence in the correlation, a larger  $R$  is needed for lower frequency modes. Therefore, the method of Thiebaux and Zwiers (1984) was used to estimate the effective degrees of freedom for each EMD mode and the corresponding correlation coefficient needed to achieve 95% confidence level. The EMD has been used in numerous studies of sea level variability (Ezer and Corlett 2012; Ezer et al. 2013; Kenigson and Han 2014; Ezer 2015; Park and Sweet 2015). In contrast with spectral analysis, EMD is a nonstationary nonparametric analysis where each mode has time-dependent amplitude and frequency, so it can detect, for example, changes of sea level rise (i.e., acceleration) over time (Ezer and Corlett 2012) or changes in oceanic kinetic energy over time (Ezer and Dangendorf 2021). EMD modes can also be combined, for example, to represent the sum of high-frequency or low-frequency oscillations, and here, the low-frequency modes provide a low-pass filtered record that filter out high-frequency variability.

### 3 Results

#### 3.1 Sea level trends and variability

The time evolutions of sea level rise in three subregions are shown in Fig. 2a, and the spatial variations in SLR are shown in Fig. 3 (the three subregions are defined in Fig. 3a). Sea level rise rate changes over the 116 years of data (Fig. 2a) and is clearly nonlinear as seen after linear detrending (Fig. 2b) with large interannual variations and an apparent ~50-year long cycle with different patterns before and after the 1960s. The sea level acceleration after the 1960s and especially in the last ~10 years of the record was well documented by many studies (Jevrejeva et al. 2008; Merrifield et al. 2009; Church and White 2011; Sallenger et al. 2012; Ezer et al. 2013; Dangendorf et al. 2017, 2019). The 3 regions are in general coherent with each other ( $R=0.75$ ), which means that ~56% of the variability is represented by all (i.e.,  $R^2=0.56$ ). However, this means that ~44% of the variability may be affected by local factors that are different in each region. Regional differences may be important for water exchange between basins (shown later); thus, Fig. 2c shows the sea level anomaly of each region relative to the whole domain (i.e., the difference between the mean SSH of each subregion and the combined mean of all three). The 3 subregions are in fact significantly anticorrelated with each other when removing the mean sea level of the whole domain ( $R$  between  $-0.1$  and  $-0.76$  with confidence level

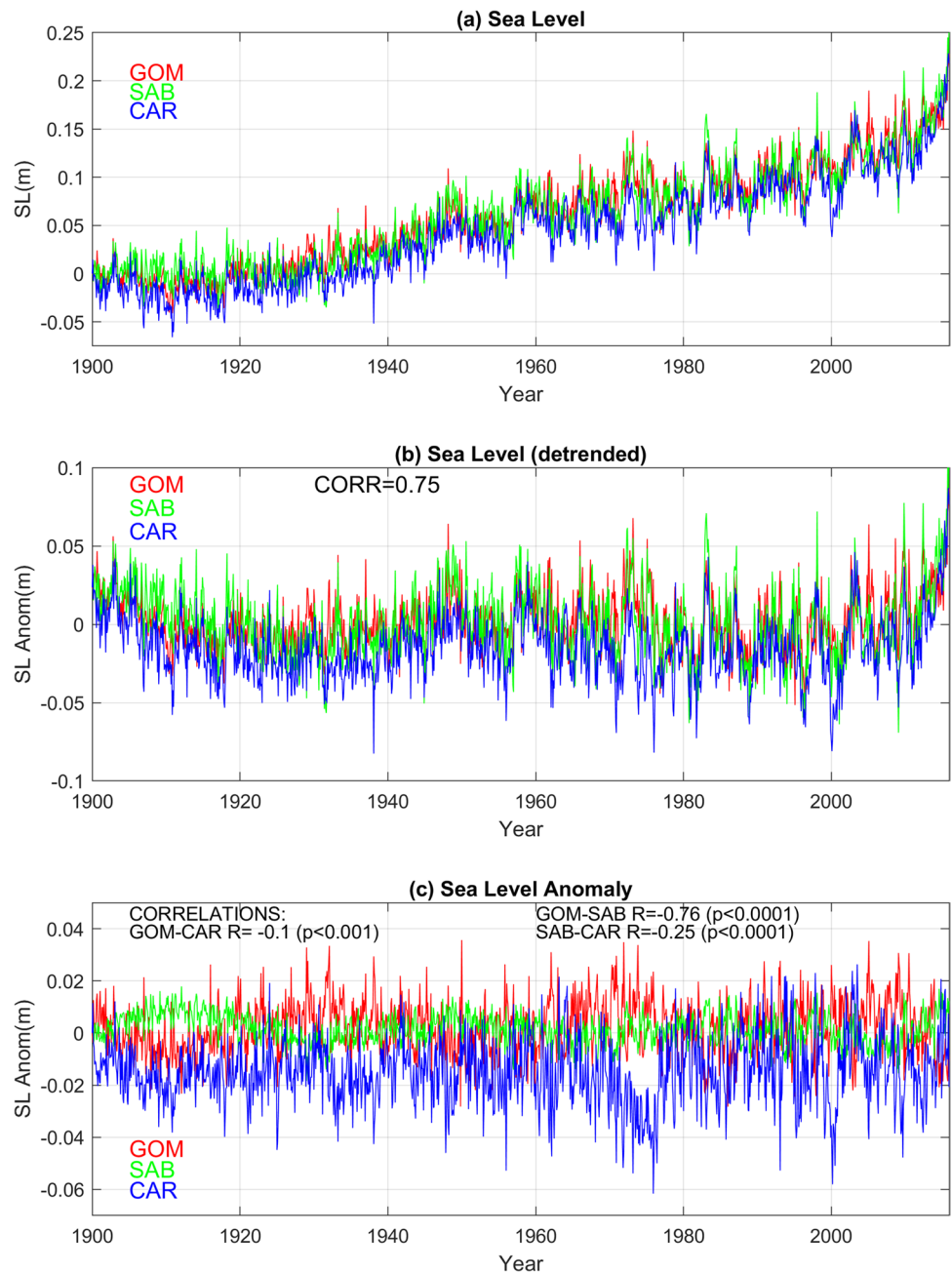
between 99.9 and 99.99%, respectively). Also note that there are some periods (the 1930s, 1970s, and ~2000) when sea level in the Caribbean Sea (CARssh in blue) decreased, while sea level elsewhere increased (GOMssh in red and SABssh in green). These regional variations in sea level will be linked later to variations in strait flows. The time series in Fig. 2 are very noisy as they include a combination of wide range of frequencies, so further analysis later with EOF and EMD will be done to investigate different spatial and temporal scales.

The recent acceleration of sea level rise, as mentioned above, is evident in the spatial pattern of sea level rise (SLR) rates (Fig. 3), with SLR less than ~1 mm/year before the 1940s (Fig. 3a) but over 4 mm/year in some locations after the 1980s (Fig. 3c). An interesting spatial pattern of SLR is an apparent shift in the location of fast SLR from the coast of the GOM during 1941–1980 (Fig. 3b) to the central GOM after 1981 (Fig. 3c). This pattern may indicate changes in ocean dynamics near strong currents, as shown for other locations (Ezer and Dangendorf 2020, 2021). For example, a shift in the Loop Current strength or position (see later) would result in sea level change due to change in the sea surface gradient across the current. Similarly, the drop of offshore sea level in the SAB at 74°W, 32°N relative to the coast (Fig. 3c), may indicate weakening of the Florida Current since the 1980s.

#### 3.2 Links between the Yucatan Channel and the Florida Strait flows and the Loop Current

The monthly velocity over the Loop Current (LCvel), in the Yucatan Channel (YCvel) and in the Florida Strait (FSvel), is shown in Fig. 4, together with their low-frequency EMD modes. Interannual variability is quite different in each location, though some periods show coherence between decadal variations in the YCvel and FSvel such as higher velocities during the 1940s, 1980s, and after 2010 and lower velocities during the 1970s; significant correlation ( $R=0.64$ ) is found between these two straits, which is not unexpected since the FS is downstream of the YC. (Note that while the correlation is statistically significant at over 99% confidence,  $R^2=0.41$  means that the correlation represents ~41% of the variability). The LCvel on the other hand is anticorrelated with the YCvel ( $R=-0.11$ ) and with the FSvel ( $R=-0.16$ ); both negative correlations are small but statistically significant at over 95% confidence level. The LCvel is also distinct from the other two currents by having a statistically significant positive trend (+3.6 cm/s per century) and increase in variability — the increased surface variability over time is a feature seen also in all western boundary currents (Ezer and Dangendorf 2021; Martínez-Moreno et al. 2021). The LC has more complex dynamics than the YC and FS flows with expansion and

**Fig. 2** Monthly reconstructed sea level (RecSL) averaged over 3 subdomains (see Fig. 3a): the Gulf of Mexico (GOM) (red), the southwestern South Atlantic Bight (SAB) (green), and the northwestern Caribbean Sea (CAR) (blue). **a** Sea level rise relative to January 1900, **b** sea level variability after removing linear trends, and **c** sea level anomaly relative to mean sea level of the entire domain of Fig. 3. Correlations between the different subregions are indicated



contraction as well as shedding of eddies (Elliott 1982; Hamilton 1992; Sturges and Leben 2000; Hamilton et al. 2002, 2014; Oey et al. 2005; Chang and Oey 2012; Hall and Leben 2016), so further analysis of the LC will be done later. It is interesting to note of two instances of extremely weak YCvel near 1940 and 2000 (Fig. 4b). This could have been just curious incidents, but fortuitously direct observations of currents in the YC that took place in 1999–2001, in fact found anomalous very low transport of ~23 Sv during this period compared with ~27 Sv in observations during later years (Athié et al. 2015, 2020); this indicates significant interannual variations, as clearly seen in Fig. 4.

The connections between the YCvel and the FSvel are examined using EMD (see Eq. 2) and shown in Fig. 5. These velocity time series produce 8 oscillating EMD modes (IMs) with mean periods ranging from ~7 months to ~47 years (even lower frequency mode 9 has incomplete cycle and neglected in Fig. 5). The YC-FS correlations are statistically significant at 95% confidence for all modes except for a cycle of ~5 years (note that the confidence level changes with frequency due to the change in degrees of freedom; see Sect. 2 for details). High significance of correlations is seen for EMD modes 1 and 4 with periods of ~7 months and ~3 years (Fig. 5a); these modes also have the highest variability in

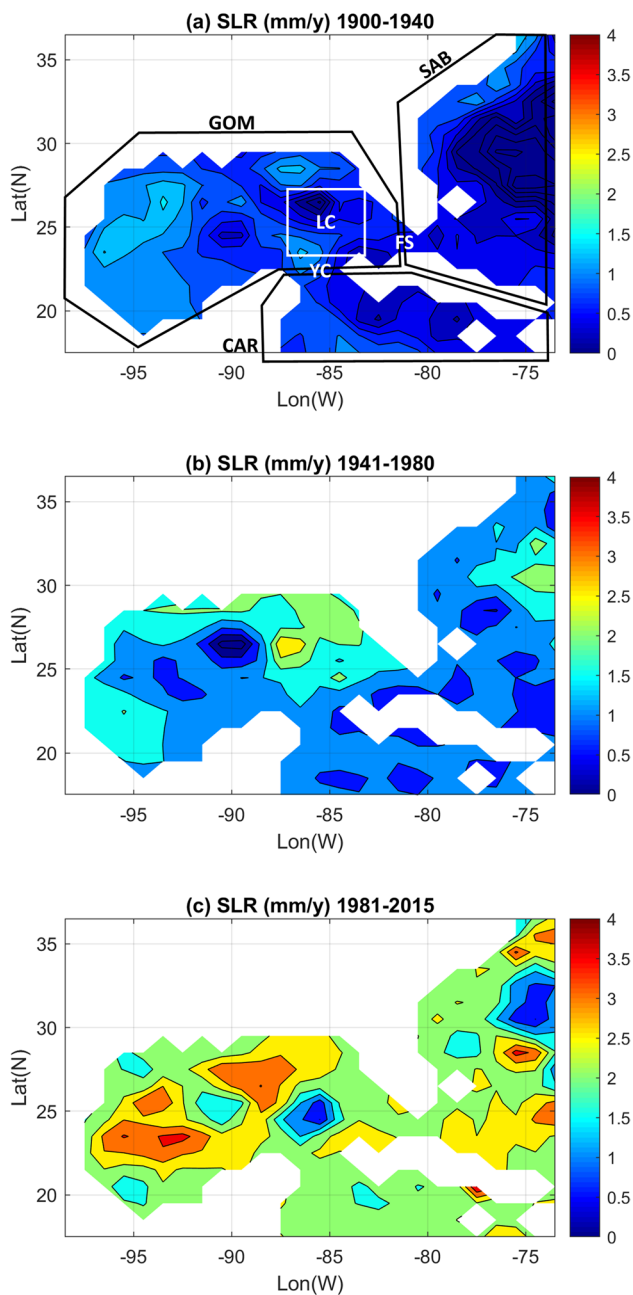


**Fig. 3** Linear sea level rise trends (in mm/y) for **a** 1900–1940, **b** 1941–1980, and **c** 1981–2015. Also shown in **a** are the 3 regions where sea level is averaged, Gulf of Mexico (GOM), South Atlantic Bight (SAB), and Caribbean Sea (CAR), and the 3 locations where current velocities were calculated: Loop Current (LC), Florida Strait (FS), and Yucatan Channel (YC)

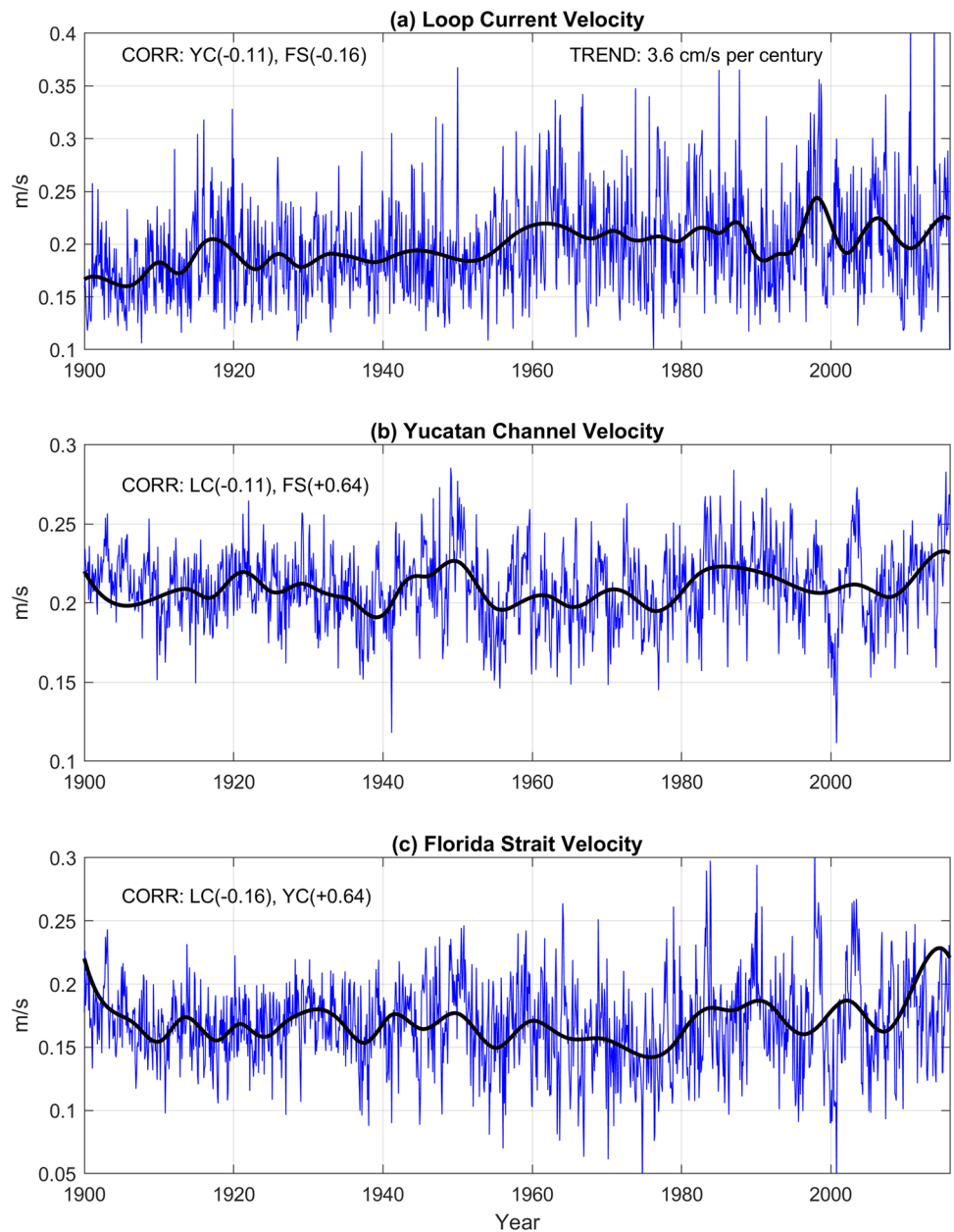
the FSvel (Fig. 5b). The percentage of variability in each mode in Fig. 5b is based on the ratio between the variance of each mode and the variance of the original time series; the values are then normalized so the sum of the variability of all 8 modes is exactly 100%. It is interesting to note that high correlations are found on both ends of the spectrum, for

high-frequency and low-frequency time scales, though the variability on those time scales is likely related to different forcing and processes, for example, mesoscale activity versus decadal climate variability. It is not clear why the EMD mode around 5-year period has reduced correlation, but at this frequency FCvel, variability significantly drops, so that YCvel variability may be linked more closely with eddy shedding rather than with FCvel. The YCvel-FSvel correlation of  $\sim 0.5$ – $0.6$  for multiannual to multidecadal periods can be compared with direct observations that cover much shorter periods and capture high-frequency variability. Candela et al. (2019), for example, found correlation of 0.83 between observed transports of the YC and the FS, for periods longer than a week, but their analysis was based on only 4 years of data, neglecting the long-term variability found here.

### 3.3 The connection between variations in ocean currents and sea level

Many studies found links between open ocean currents and coastal sea level (Blaha 1984; Ezer et al. 2013; Yin and Goddard 2013; Goddard et al. 2015; Park and Sweet 2015; Ezer 2015; Dangendorf et al. 2021), especially near strong flows such as the Gulf Stream and its upstream branch, the Florida Current. However, much less attention has been given to the potential influence of the Loop Current on sea level along the GOM coast. As other strong ocean currents in the northern hemisphere that are near geostrophic balance, the LC has higher sea level on the right of the flow and lower sea level on the left, which can be seen even in the coarse-resolution RecSL data (Fig. 6a). Therefore, variations in strength or position of the LC are expected to influence sea level on both sides of the current. The linear correlation coefficients between sea surface height time series (after removing linear trends) at each point in the domain and the time series of the 3 velocities are shown in Fig. 6b–d. The correlation of sea level with LCvel (Fig. 6b) shows a 3-lobe positive–negative–positive pattern near the LC, so that increased LC velocity is associated with decreased sea level north of the current. The northwestern coasts of the GOM have negative correlations, suggesting that weakening LCvel may cause coastal sea level rise, as seen along the Gulf Stream (Ezer et al. 2013). The correlation of sea level with YCvel (Fig. 6c) and with FSvel (Fig. 6d) is quite similar and consistent with the geostrophic balance that dictates larger sea level gradients when flow increases. Both cases further emphasize that climate-related weakening in the current will raise sea level along the majority of the GOM and SAB coasts. The strongest impact (and negative correlation) is seen along the southwestern Florida coast and along the coasts of the SAB from Florida to North Carolina. One apparent difference between the impact of YCvel and FSvel is seen in the Caribbean Sea where stronger YCvel seems to be linked with a northward

**Fig. 4** Mean geostrophic velocity speed over **a** the Loop Current (24°N–28°N, 83°W–87°W), **b** across the Yucatan Channel (23°N), and **c** across the Florida Strait (81°W); see Fig. 3a for locations. Blue lines are monthly values, and black heavy lines are low-frequency EMD modes. Significant correlations and trends are indicated (only **a** has significant upward trend)



shift of the Caribbean Current (Fig. 6c). While many studies, mentioned before, link the coastal sea level along the SAB with the nearby Florida Current transport measured off the east coast of Florida (Baringer and Larsen 2001; Meinen et al. 2010), here, it is shown that currents farther upstream, all the way back to the YC, are also linked with coastal sea level in the SAB (and possibly farther downstream along the Gulf Stream).

The spatial patterns of correlations in Fig. 6 suggest that sea level variations in the GOM are quite different at different locations around the LC; therefore, EOF analysis of SSH is conducted to assess spatial and temporal patterns (Fig. 7). Almost 60% of the variability is captured by the first 5 EOF modes with spatial patterns (left panels of Fig. 7) centered

mostly around the LC. EOF-1, for example, indicates (top panel) that when sea level decreased in the LC area, sea level in the rest of the GOM and most of the SAB will rise. It is interesting to note that the pattern of EOF-1 that captured 23% of the RecSL SSH variability resembles the pattern of the first EOF calculated from low-pass filtered altimeter data that captured 29% of the variability (see Fig. 3a in Lin et al. (2010)). The time evolution of the EOF modes (right panels of Fig. 7; the PCs in Eq. 1) indicates nonstationary oscillations that includes both high-frequency interannual variations and decadal and multidecadal changes. For example, the analysis may indicate a potential large change in the strength of the LC between the 1960s and 1980s (EOF-1) and changes in the sea level on the coast of the western

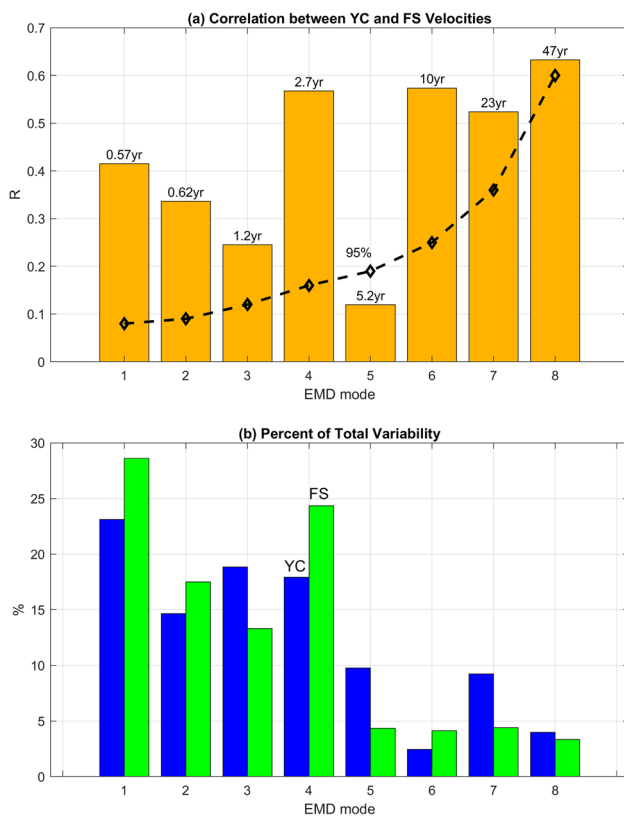


**Fig. 5** The relation between the Yucatan Channel (YC) flow and the Florida Strait (FS) flow. **a** FS–YC correlation of each EMD oscillating mode; the average period of each mode is indicated on top of each bar. The dash line represents estimated 95% confidence level based on the loss of degrees of freedom with decreasing frequency (see text). **b** Percent of total variability captured by each EMD mode for the YC and FS flows in blue and green bars, respectively

GOM during the 1950s (EOF-5). Since the variations of sea level are correlated with variations in velocity (Fig. 6), an attempt is made to see which PC mode in Fig. 7 is related to which velocity (YCvel, LCvel, or FSvel) and moreover, if there is a sea level velocity connection, to find at what time scales they exist. To do such a comparison, the EMD modes of the PCs in Fig. 7 are compared with the EMD modes of the velocities of Fig. 4, and the cross-correlations are calculated for the combined high-frequency EMD modes and low-frequency EMD modes.

The results show that EOF-1 (top panel of Fig. 7) is significantly correlated with the YCvel (Fig. 8), with correlation of  $R=0.35$  and  $0.56$  for the high- and low-frequency EMD modes, respectively. The low-frequency modes show a cycle with a period of  $\sim 25$  years, though during the 1970s to the 1990s the two time series lost some coherence between them. The fact that variations in the YC velocity impact the LC (and EOF-1) is consistent with Fig. 6 and the dynamics of the GOM as suggested by past studies (Maul et al. 1985; Bunge et al. 2002; Candela et al. 2003; Oey 2004;

Oey et al. 2005; Lin et al. 2010). For example, Lin et al. (2010) compared the observed YC flow during September 1999 to May 2001 to low-pass filtered SSH in the LC area and found correlation of 0.8, but the observations were too short to be conclusive.

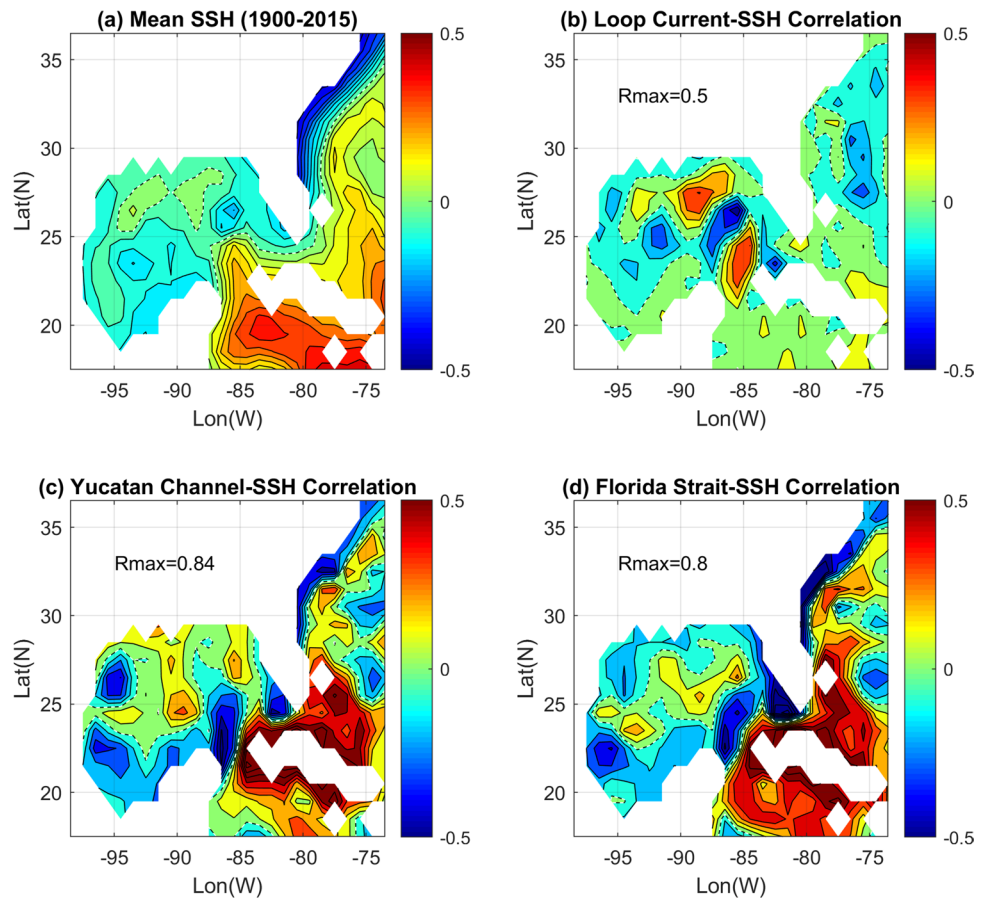
EOF-2, EOF-3, and EOF4 have similar spatial pattern, and their combined time series was found to correlate best with the LC velocity (Fig. 9), but unlike EOF-1 that had higher correlation at low frequencies, EOF-234 has higher correlation with the LCvel at high frequency ( $R=0.59$ ) than low frequency ( $R=0.52$ ); both correlations are significant at over 95%. The high-frequency oscillations have time scale of  $\sim 5$  years and the low frequency  $\sim 25$  years. These EOF modes may relate to shifting in the extent of the LC and shedding of eddies with high variability extending from the LC westward (in particular, see EOF-4 in Fig. 7).

Finally, the combined EOF-4 and EOF-5 are best correlated with the FSvel (Fig. 10), with correlation of  $R=0.56$  for both high- and low-frequency modes. In this case, there is apparent increase in variability over time (see left panels of Fig. 10), which may relate to the general increase in kinetic energy of all western boundary currents as pointed by Ezer and Dangendorf (2021, 2022). The cross-correlation indicates cycles with periods of  $\sim 10$  years and  $\sim 50$  years and increased multidecadal oscillations since the 1980s. The results here are consistent with the results of Lin et al. (2010) who compared the low-pass filtered SSH altimeter data over the LC with the observed cable measurements of the Florida Current and found correlations of 0.45 that were statistically significant at 99%.

### 3.4 Sea level, the Loop Current, and the North Atlantic Oscillations (NAO)

The mean sea level in the Caribbean Sea shows some periods with a peculiar large difference with the mean sea level over the GOM (Fig. 2c); this is especially apparent during the 1970s and around 2000, when CARssh dropped relative to the GOMssh. To investigate possible connections between these regional variations in sea level and large-scale climate variability, the difference between the GOMssh and the CARssh (hereafter, “SLdif”) is compared with the annual NAO index in Fig. 11. During the 116 years of RecSL, the largest change occurred when SLdif increased between the 1950s and 1970s and then decreased between the 1970s and 1990s (Fig. 11b). At the same time, NAO index decreased and then increased (Fig. 11a). In fact, several past studies focused on unusual changes observed in the North Atlantic between the 1950s and 1970s (though at the time these studies did not link those changes to the NAO). For example, from hydrographic data, Levitus (1989) found large difference in the temperature and salinity climatology of the Atlantic Ocean

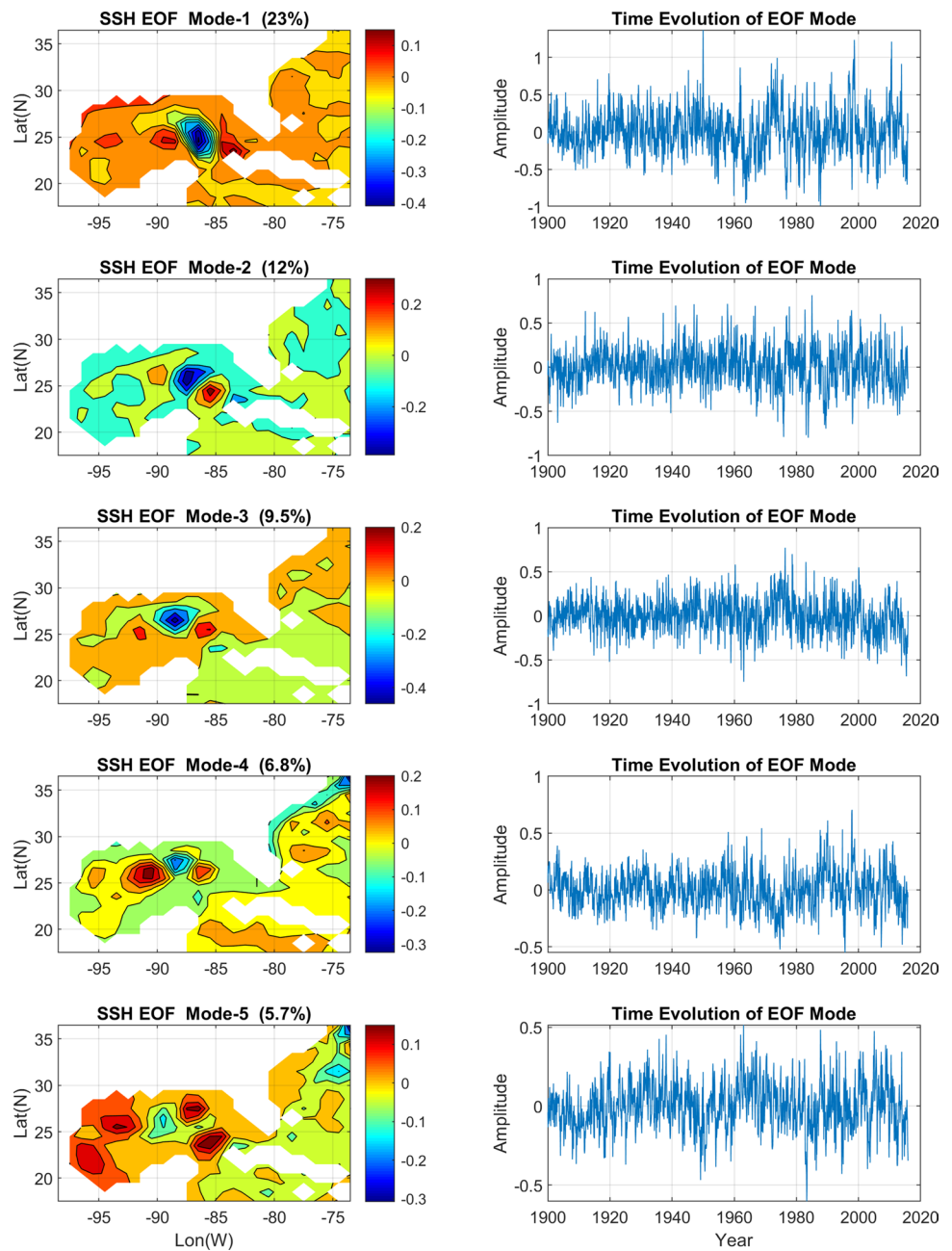
**Fig. 6** **a** Mean sea surface height (SSH) of the RecSL data. **b**, **c**, and **d** are the correlations of detrended SSH time series at each grid point with the flow of the LC, YC, and FS (Fig. 4), respectively. Dash contours are zero correlation lines, separating positive (red) and negative (blue) correlations. Rmax is the maximum correlation value; correlations with  $|R| > 0.08$  are statistically significant at the 95% confidence level



between 1955–1959 and 1970–1974, and using models, Greatbatch et al. (1991) found a large decrease in the Gulf Stream transport, and Ezer et al. (1995) found significant increase in sea level along the US coast and weakening in AMOC (Ezer 2015) for the same periods. Using ocean models, Blaker et al. (2014) also reported on an unusually low NAO and a weaker AMOC during the 1970s, with similarity to atmospheric conditions during 2009–2010 when unusually weak AMOC was observed (extremely low NAO is also seen around 2010 in Fig. 11a). While AMOC and NAO have been linked to recent coastal sea changes along the US East Coast (Little et al. 2019; Ezer 2015), to our knowledge, this is the first time that the large change in the Atlantic Ocean during the 1970s was linked with sea level in the GOM. Weakening in the trade winds and slowing down in the AMOC circulation may have affected the Caribbean Sea as shown here. In the recent decade, one notes the largest negative peak in NAO around 2010 which was linked with unusual weakening AMOC and increased coastal sea level along the US East Coast (Blaker et al. 2014; Ezer 2015; Goddard et al. 2015), while during 2010–2015, NAO and SLdiff again move in opposite direction (Fig. 11).

In addition to the multidecadal change discussed above, the SLdif shows several unusual low and high peaks (highlighted in Fig. 11b by dates and red circles). Surprisingly, almost all the minima peaks occurred in October (from 1949 to 2014), and most of the high peaks occurred around January to February (from 1938 to 2005), indicating a potential seasonal pattern (see discussion on the seasonal pattern later). Keep in mind, however, that RecSL excludes seasonal variations in sea level, so these are likely variations in ocean dynamics. Looking at the AVISO, altimeter data during those peaks indicates a particular pattern in the LC, and a few examples are shown in Fig. 12. Most of the minima peaks in Fig. 11b (in October) have retracted LC, sometimes after shedding an eddy (Fig. 12a, c), while most of the maxima peaks in Fig. 11b (in January to February) have LC that is extended farther north, sometimes before shedding an eddy (Fig. 12b, d). Other images (not shown) are quite similar. This pattern can be explained by the fact that when the LC extended farther into the GOM, the area occupied by the warmer LC waters increases, and this expansion must be compensated by increased flow through the YC toward the GOM.

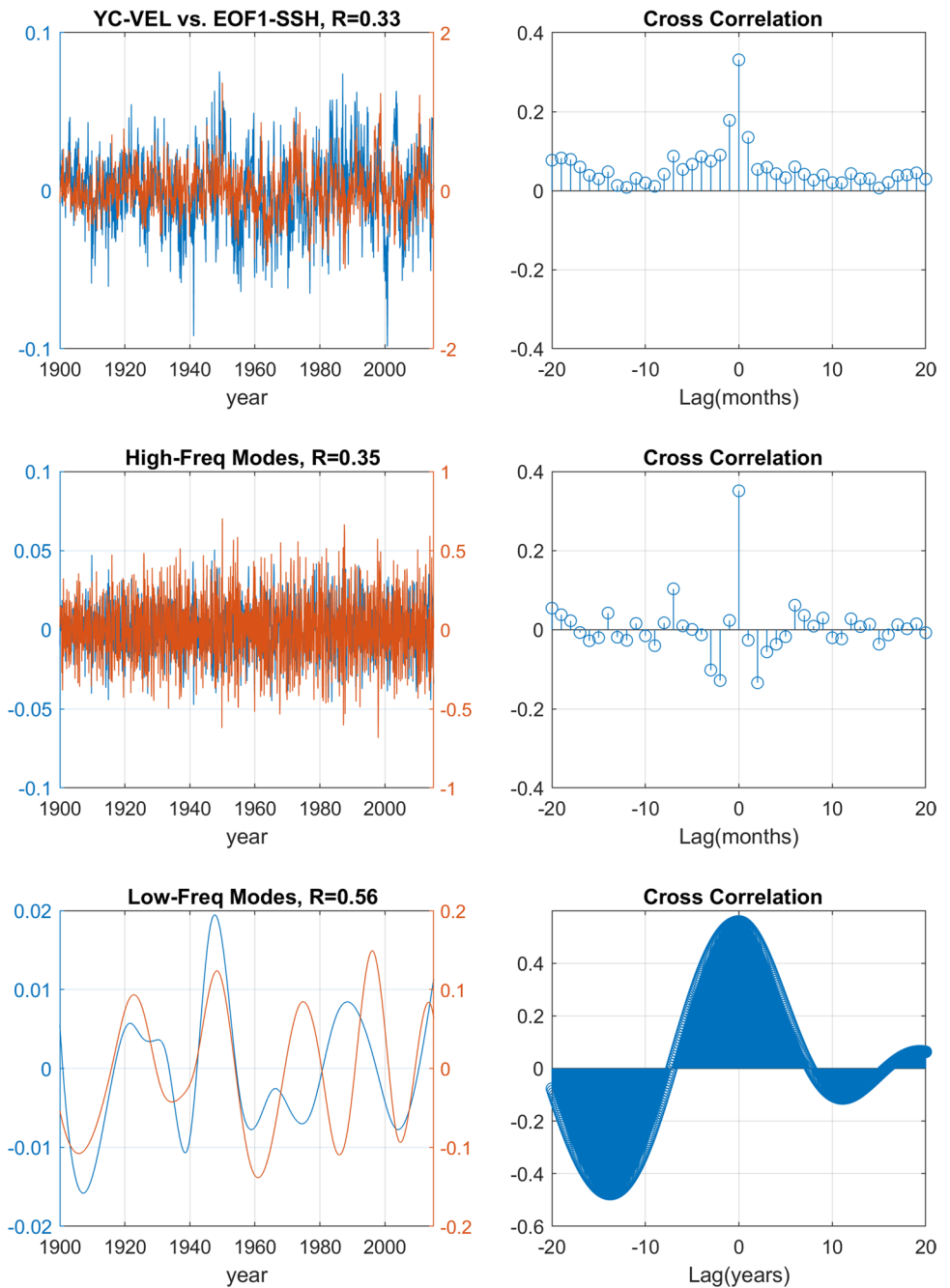
**Fig. 7** The first 5 spatial modes of empirical orthogonal function (EOF) analysis of SSH (left columns) and their time evolution (right columns); percentage of total variability is indicated on the left panels. Note that different scales are used in each panel to better show the pattern in each mode



Continuous quantitative data on the extension of the LC became available during the altimeter era (since 1993, excluding the more sparse data during the earlier satellite altimeters of Seasat and Geosat). The monthly mean total area of the LC reported by Hamilton et al. (2014) during 1993–2012 looks remarkably like the seasonal pattern of the YC velocity obtained from the RecSL for 1900–2015 (Fig. 13a); the correlation between the two data sets  $R=0.63$  has confidence level of 98%. Two high peaks in both YCvel and LC extension are found in February and June, while the minimum observed LC area in October coincides with the periods of retracted LC (Fig. 11b and Fig. 12a and c).

There is a long history of research trying to connect the flow through the YC with the extension of the LC and trying to find explanations for the seasonal pattern of the LC, with sometimes contradicting results (Maul 1977; Maul et al. 1985; Sturges and Leben 2000; Bunge et al. 2002; Candela et al. 2003, 2019; Oey 2004; Oey et al. 2005; Chang and Oey 2012; Hamilton et al. 2014; Hall and Leben 2016; Athié et al. 2020). It is especially difficult to detect a seasonal cycle in eddy shedding from the LC, because of the irregular timing between shedding events, the long period between such events, and the fact that satellite altimeter data only covers a few decades. Therefore, the long record of RecSL provides

**Fig. 8** Comparison between the time evolution of SSH EOF1 (top-right panel of Fig. 7) and the YC velocity (Fig. 4b, after removing the mean); right panels are cross-correlations. Top panels are the original monthly time series, middle panels are combined high-frequency EMD modes, and bottom panels are the combined low-frequency modes

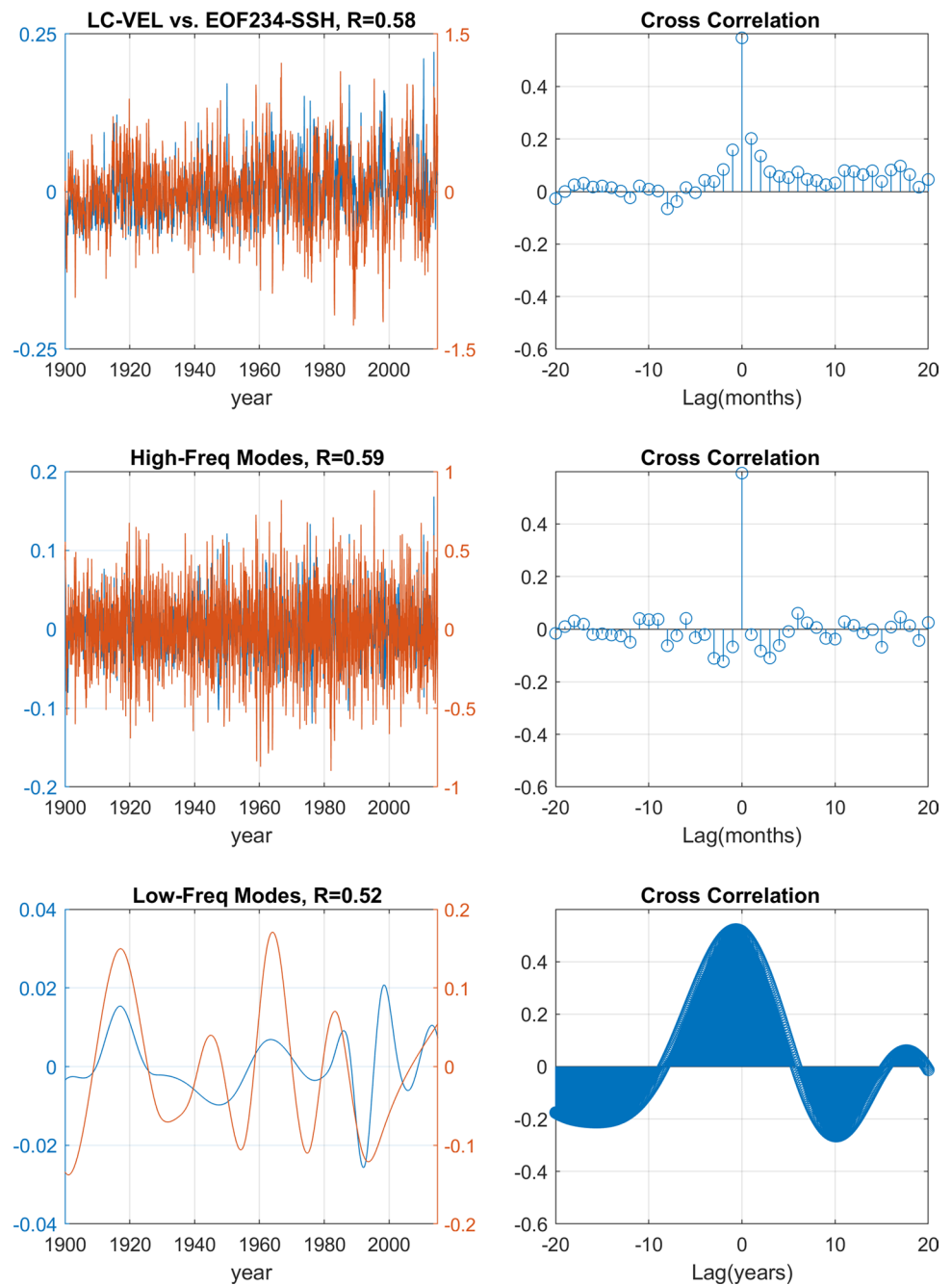


further evidence for the existence and cause of the seasonal cycle in the LC system.

In contrast with the long RecSL record of 116 years, direct observations of the YC transport started in the late 1990 (Bunge et al. 2002; Sheinbaum et al. 2002; Candela et al. 2003, 2019) and are relatively short. Analyzing ~5 years of direct measurements, Athié et al. (2020) found a seasonal cycle in the YC transport with maximum transport in the summer (July to August). However, the minimum transport of the observations was in March, which contradicts altimeter data that had minimum in November. The comparison of the YCvel from

the RecSL with Athié et al.’s observations of the YC transport (Fig. 13b) shows generally similar pattern but correlation of only 0.45 (90% confidence level); the relatively low correlation is likely due to the different between the two time series in the month of maximum flow. Coincidentally, the maximum YC flow from the RecSL data in June is at the same month as obtained by 3 years of early hydrographic observations (Molinari et al. 1978), while the recent 5-year observations (Athié et al. 2020) indicated maximum in July to August. The RecSL data indicates minimum flow in November to December, more like the longer record of the altimeter data than the direct but

**Fig. 9** Same as Fig. 8, but for comparison between the LC velocity (Fig. 4a) and combined EOF modes 2–4 of SSH (Fig. 7)



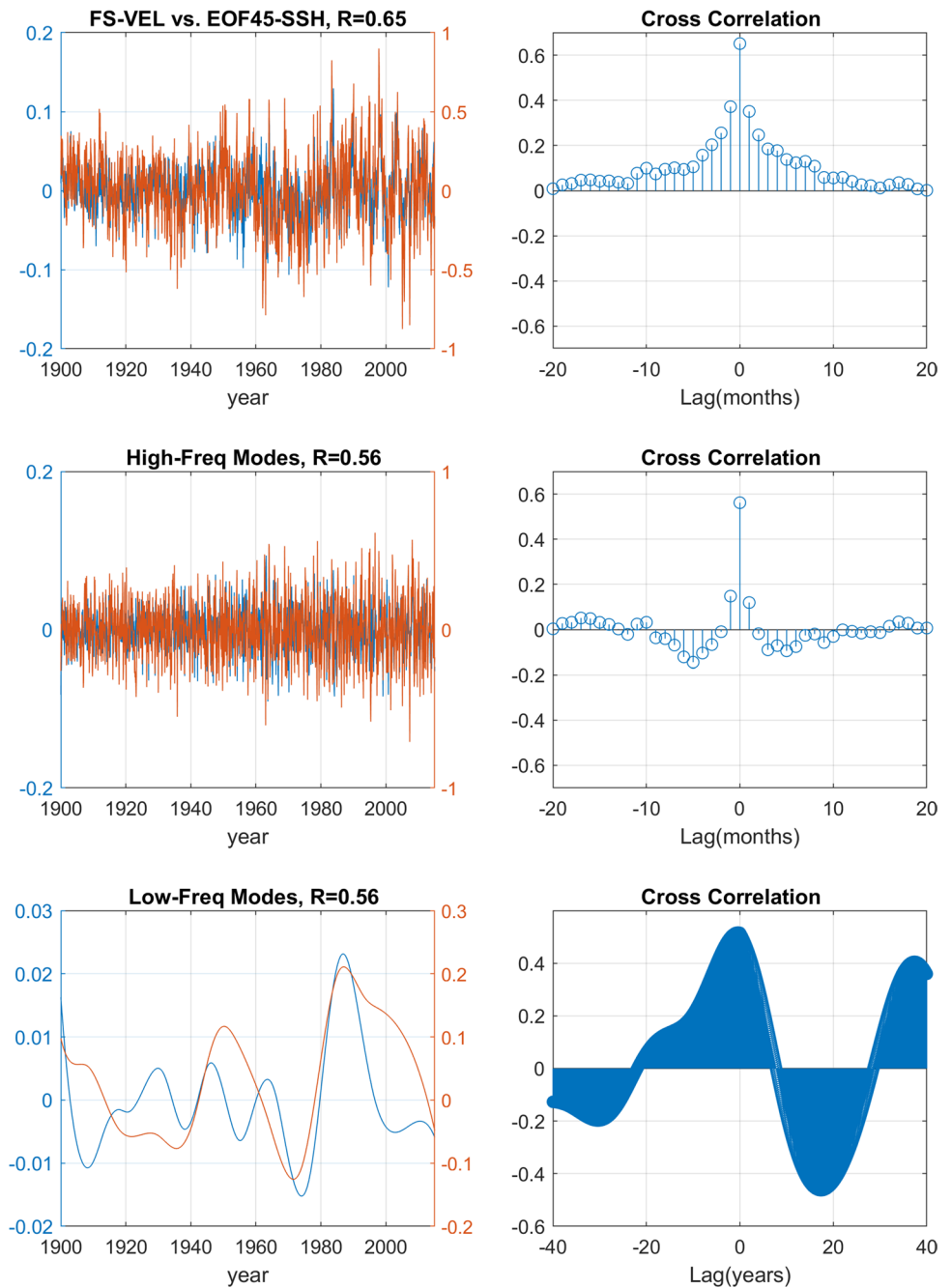
short-term observations. Moreover, the correlation between the observed LC extension (red line in Fig. 13a) and the seasonal cycle obtained from the 4-year direct YC observations (red line in Fig. 13b) is not statistically significant ( $R=0.2$ ), compared with the higher correlation ( $R=0.63$ ) obtained between the LC area and the 116 years of YCvel from the RecSL data. What this comparison demonstrates is that there is likely a seasonal cycle in the LC and in the flow through the YC and the FS, and there is a clear connection between those currents, as previous studies had shown. However, the interannual and decadal variations are much larger than the seasonal

signal, as can be seen in Fig. 4, so that different data sources and different data periods would likely result in somewhat different seasonal cycle.

## 4 Summary and conclusions

The study follows on the footsteps of recent research (Dangendorf et al. 2019, 2021; Ezer and Dangendorf 2020, 2021, 2022; Frederikse et al. 2020; Gehrels et al. 2020) that used sea level reconstruction (RecSL) to study sea level rise and

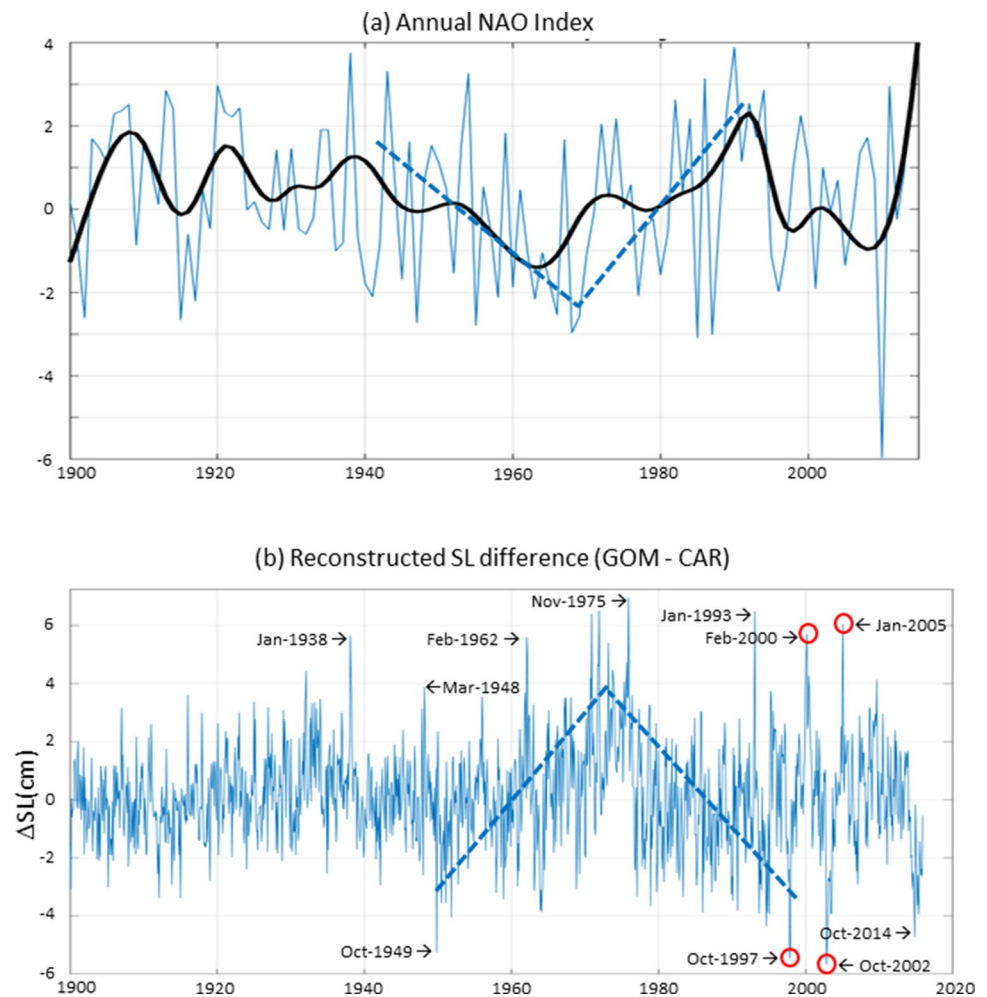
**Fig. 10** Same as Fig. 8, but for comparison between the FS velocity (Fig. 4c) and the combined EOF modes 4–5 of SSH (Fig. 7)



connections between open ocean dynamics and variations in coastal sea level. Such studies are important, for example, for addressing risks for coastal communities under threat of sea level rise and impacts of climate change. The relatively low spatial resolution ( $1^\circ \times 1^\circ$ ) of the RecSL data cannot resolve mesoscales and smaller features, such as the details of the LC. However, it is a global data set with a long record (116 years  $\times$  12 monthly data = 1392 data points at each latitude/longitude location), so it can detect decadal and multi-decadal variability and their regional patterns, a task that is impossible to achieve with direct observations which are

often much shorter in duration. Regions with strong flows like western boundary currents (WBCs) or the LC in the GOM have sufficient sea level gradients to calculate surface geostrophic currents even from the coarse-resolution RecSL data. Therefore, climatic changes in ocean dynamics such as weakening in the Gulf Stream flow (Ezer and Dangendorf 2020) and increased surface oceanic kinetic energy over WBCs and the global ocean (Ezer and Dangendorf 2021, 2022) could be detected with this data while filtering out high-frequency oscillations and small-scale variability. The Gulf of Mexico plays an important role in the path of the

**Fig. 11** **a** The North Atlantic Oscillation (NAO) index, showing annual means (blue) and low-pass filtered (black). **b** Monthly sea level difference between the GOM and the CAR regions (Fig. 2c). Blue dash heavy lines in **a** and **b** indicate a period of large multidecadal change. The times of some extreme sea level difference are marked in **b**; red circles indicate the time of the altimeter data shown in Fig. 12

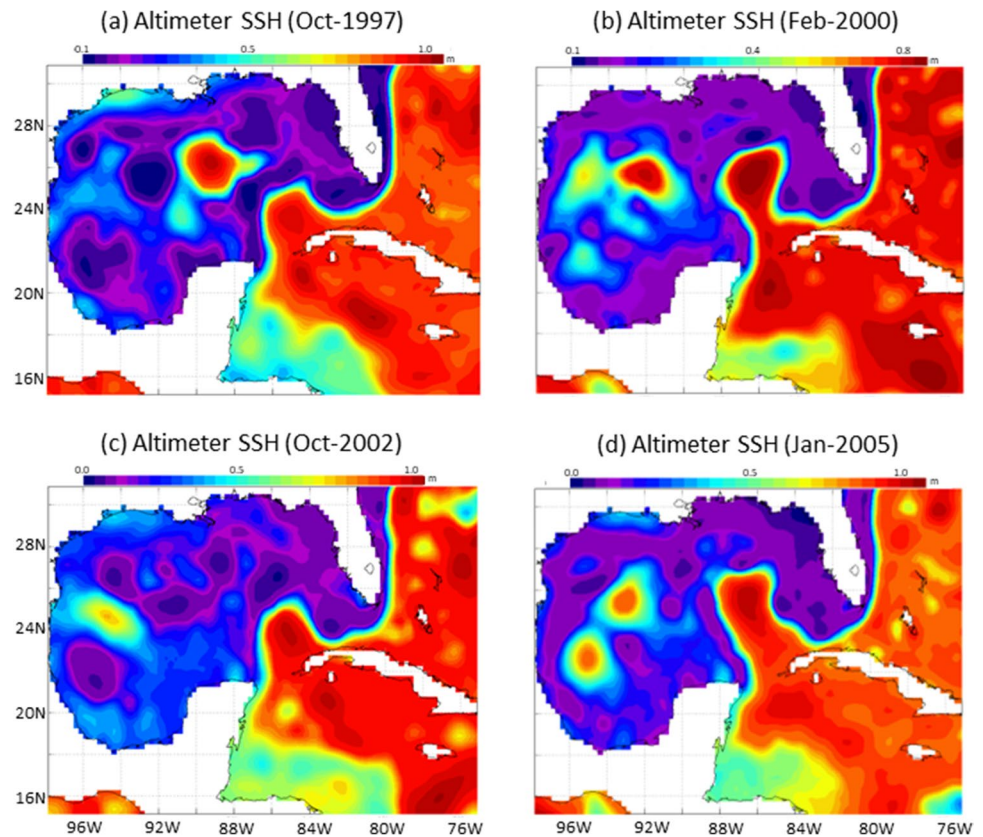


WBC of the Atlantic Ocean that includes the Caribbean Current, the Loop Current, the Florida Current, and the Gulf Stream. These are strong currents with variabilities on a wide range of scales, from daily and monthly to multidecadal. Therefore, the goal of the study was to look at variations around the GOM region using a longer record than any direct observations, to better understand mechanisms and drivers of ocean dynamics in and around the GOM.

The Gulf of Mexico has been studied extensively over many years since the early hydrographic observations (Reid 1972; Maul 1977; Molinari et al. 1978; Vukovich et al. 1979; Elliott 1982; Sturges and Evans 1983; Maul et al. 1985), but continuous observations in the region are relatively short. Florida Current transport measurements started in the early 1980s (Baringer and Larsen 2001; Meinen et al. 2010), significant altimeter data in the early 1990s (Ducet et al. 2000), and measurements of the flow in the entire Yucatan Channel started in the late 1990s but with considerable gaps (Bunge et al. 2002; Sheinbaum et al. 2002; Candela et al. 2003; 2019; Athié et al. 2020), providing up to  $\sim 5$  years of continuous measurements.

Very little oceanic information was available in much of the GOM during the first two third of the twentieth century. Therefore, having the RecSL record since 1900 allows to study variability on longer time scales than previously was possible, and indeed, this study found, for example, large climatic changes in the GOM during the 1970s; previously, large climatic changes during this period were only described in the North Atlantic basin (Levitus 1989), with some similarity to recent changes associated with weakening AMOC (Ezer 2015). Having a long record is especially important for studies of the LC eddy shedding because these events are unpredictable and infrequent. For example, Sturges and Leben (2000) detected 34 eddy separation events between 1973 and 1999 with typical separation periods of 6–11 months; Hamilton et al. (2014) further discussed the difficulty of identifying eddy separation in different data sets and different models. This long period between eddy shedding events, that is, close to annual but not quite the same, can create aliasing and difficulty in studying the seasonal cycle in the GOM and any long-term variability that is dominated by the LC dynamics.

**Fig. 12** Gridded AVISO SSH altimeter data for the 4 periods indicated by red circles in Fig. 11b

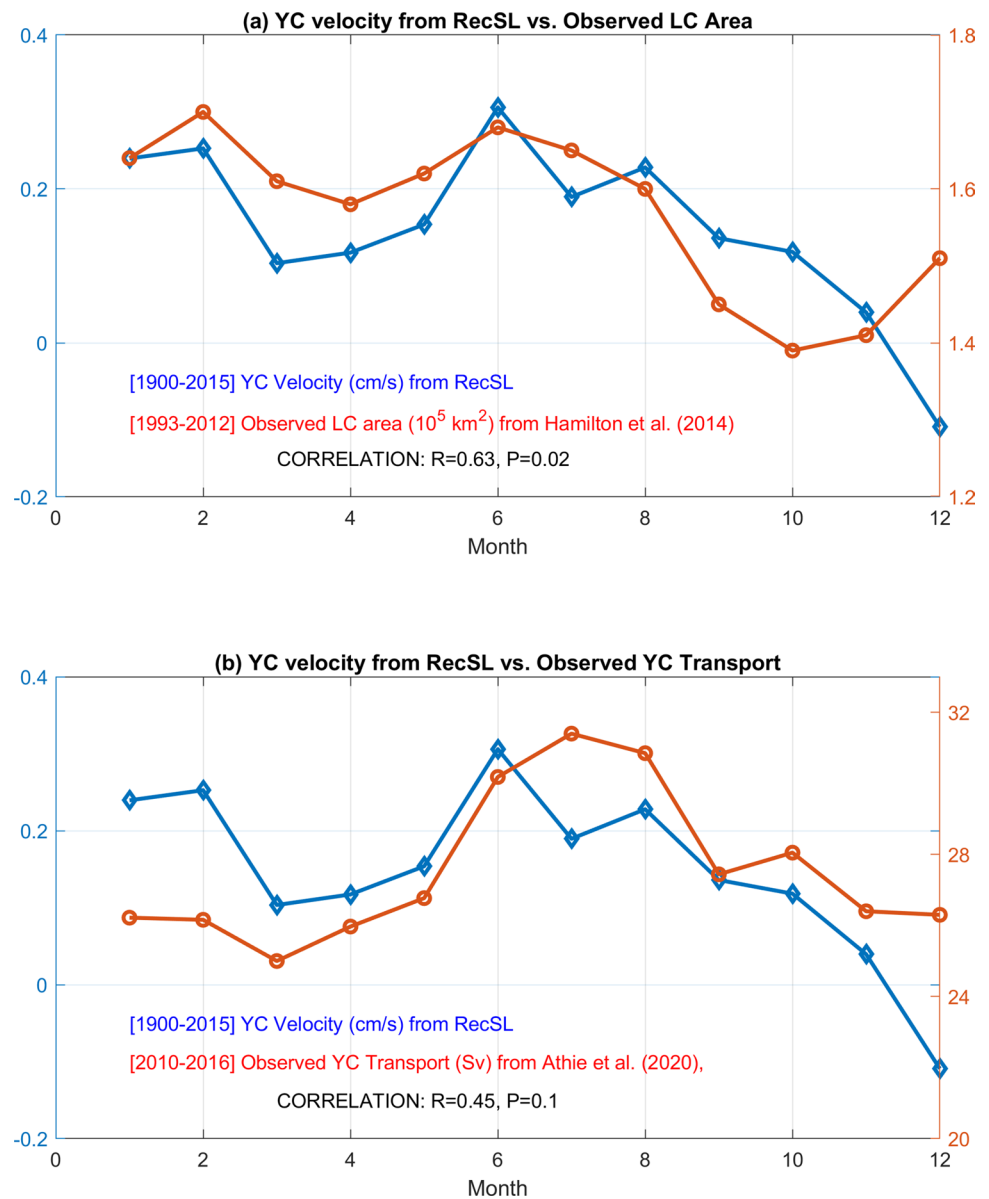


The results show that while sea level in the GOM region is rising and accelerating in recent decades, there are significant regional variations that indicates dynamic shifts rather than coherent regional sea level rise. For example, compared with the past, say before the 1980s when sea level rose relatively slowly ( $\sim 1\text{--}2$  mm/y) but faster near the GOM coasts, in recent decades, sea level rose much faster in the interior of the GOM ( $\sim 3\text{--}4$  mm/year) than along the coast; this indicates potential climatic changes in the warming and the dynamics of the LC. Indeed, the record shows that over the past century, the LC experienced increased surface flow and increased variability, which is consistent with the increased surface kinetic energy seen in all WBCs (Ezer and Dangendorf 2021). It was suggested by the latter study that uneven ocean warming causes increased kinetic energy, and in this case, warmer waters entering from the Caribbean Sea into the LC would increase surface gradients relative to cooler waters outside the LC, thus strengthening the currents. Another goal of the study was to link the inflow/outflow through the YC/FS with the dynamics inside the GOM. While the flows of the two straits are significantly correlated with each other for time scales from few months to  $\sim 50$  years as seen by an EMD analysis, the relation explains only  $\sim 50\%$  of the variability, so differences between inflow and outflow may be related to variations in the extension of the LC, as suggested by Maul et al. (1985)

and later others. Unfortunately, Maul's one current meter data at the YC sill was insufficient to prove the relation between the YC flow and the LC, but later observations and models did find connections (Bunge et al. 2002; Oey 2004; Oey et al. 2004, 2005; Lin et al. 2010; Candela et al. 2019). The results here, using much longer records of any of the above studies, indeed confirm the close links between the flow of the YC and the FS and variations in the LC; however, this relation is not only complex but can affect sea level over the entire GOM on time scales ranging from few months to few decades. The first EOF mode of SSH in the GOM (23% of the variability) is indeed correlated with the YC flow, while higher modes are correlated with the FS flow and the velocity of the LC itself.

The record of sea level difference between the GOM and the northern Caribbean Sea shows interesting results and can provide an indicator for dynamic variations on different time scales. On long-term time scales, one unusual period during the 1970s with large sea level difference stands out in the 116-year record (the change started in the 1950s and ended in the late 1990s). This period of large sea level difference between the two basins coincides with a period of low NAO, large changes in subsurface temperatures in the North Atlantic Ocean and significant slowdown of the GS and AMOC (Levitus 1989; Greatbatch et al. 1991; Ezer et al. 1995; Ezer 2015). A combination of weakening trade winds

**Fig. 13** Seasonal cycle in different observations: a comparison between the monthly mean YC velocity (blue, in cm/s, left axis) obtained from the RecSL and monthly mean observations (red, right axis). **a** Observed Loop Current area (in  $10^5 \text{ km}^2$ ) obtained from altimeter data (Hamilton et al. 2014) and **b** observed YC transport from direct mounted measurements (Athié et al. 2020). The period of each data is indicated (“[]”) as well as the correlation



and weakening circulation in the North Atlantic Ocean may have contributed to this change. On short-term time scales, extreme peaks in sea level difference seem to detect variations in the LC extension with high/low peaks occurring over extended/retracted LC. Therefore, the results show that variations in the LC are linked with large-scale variations in sea level beyond the GOM. On seasonal time scales, the analysis found that the seasonal variations in the YC flow obtained from RecSL are significantly correlated ( $R=0.63$ ) with the extension of the LC obtained from recent altimeter data (Hamilton et al. 2014), confirming early suggestions that larger flow through the YC is linked with extended LC area. However, a comparison between the seasonal cycle of RecSL-derived YC flow and the seasonal cycle obtained from direct measurements of YC transport over ~5-year

period (Athié et al. 2020) was only marginally significantly correlated ( $R=0.45$ ), showing the need for very long observed record to account for the interannual and decadal variability which dominated the region. Early studies suggest that the seasonal wind pattern may drive the seasonality of the LC (Sturges and Evans 1983), but it was obviously very difficult to detect the seasonal cycle of the LC from limited observations of the time. Recent studies using more data and models confirm that increased trade winds over the Caribbean Sea during summer and winter increased the YC transport, which consequently increased the LC intrusion into the GOM and increased the likelihood of eddy shedding (Chang and Oey 2012; Athié et al. 2020). The two peaks in YC flow seen in the analysis here in February and June (Fig. 13) thus agree very well with the recent studies.

In summary, the study shows the usefulness of the century-long RecSL record to detect changes in ocean dynamics over longer time scales than was previously possible with direct observations. Analyzing a long record is especially critical in a region like the GOM where processes such as LC eddy shedding are infrequent with long intervals between events. Comparisons with recent observations reaffirm that dynamic surface currents obtained from coarse-resolution sea level reconstruction can capture quite well long-term variations in ocean dynamics of major ocean currents; it is hoped that sea level reconstruction with higher resolution will soon be available to allow studying of long-term mesoscale and sub-mesoscale variabilities.

**Acknowledgements** The study is part of Old Dominion University's Climate Change and Sea Level Rise Initiative at the Institute for Coastal Adaptation and Resilience (ICAR). The Center for Coastal Physical Oceanography (CCPO) provided facility and computational resources. S. Dangendorf is thanked for providing the sea level reconstruction data. Two anonymous reviewers are thanked for useful suggestions that helped to improve the manuscript.

**Data availability** The NAO index is available from UCAR (<https://climatedataguide.ucar.edu/climate-data/hurrell-north-atlantic-oscillation-nao-index-pc-based>), the altimeter data is available from AVISO (<http://las.aviso.oceanobs.com/>), or the Copernicus Marine service (<https://marine.copernicus.eu/>), and the RecSL data is available by request from the author. The data used are publicly available from the links provided and the reconstruction is available by request from the author.

## Declarations

**Conflict of interest** The author declares no competing interests.

## References

- Athié G, Sheinbaum J, Leben R, Ochoa J, Shannon MR, Candela J (2015) Interannual variability in the Yucatan Channel flow. *Geophys Res Lett* 42:1496–1503. <https://doi.org/10.1002/2014GL026274>
- Athié G, Sheinbaum J, Candela J, Ochoa J, Pérez-Brunius P, Romero-Arteaga A (2020) Seasonal variability of the transport through the Yucatan Channel from observations. *J Phys Oceanogr* 50(2):343–360. <https://doi.org/10.1175/JPO-D-18-0269.1>
- Baringer MO, Larsen JC (2001) Sixteen years of Florida Current transport at 27°N. *Geophys Res Lett* 28(16):3179–3182. <https://doi.org/10.1029/2001GL013246>
- Beyer J, Trannum HC, Bakke T, Hodson PV, Collier TK (2016) Environmental effects of the Deepwater Horizon oil spill: a review. *Mar Poll Bull* 110(1):28–51. <https://doi.org/10.1016/j.marpolbul.2016.06.027>
- Blaħa JP (1984) Fluctuations of monthly sea level as related to the intensity of the Gulf Stream from Key West to Norfolk. *J Geophys Res* 89:8033–8042. <https://doi.org/10.1029/JC089iC05p08033>
- Blaker ET, Hirschi JM, McCarthy G, Sinha B, Taws S, Marsh R, Coward A, de Cuevas B (2014) Historical analogues of the recent extreme minima observed in the Atlantic meridional overturning circulation at 26°N. *Clim Dyn* 44(1–2):457–473. <https://doi.org/10.1007/s00382-014-2274-6>
- Blumberg AF, Mellor GL (1985) A simulation of the circulation in the Gulf of Mexico. *Isr J Earth Sci* 34:122–144
- Bretherton CS, Smith C, Wallace JM (1992) An intercomparison of methods for finding coupled patterns in climate data. *J Clim* 5:541–560. [https://doi.org/10.1175/1520-0442\(1992\)005%3c0541:AIOMFF%3e2.0.CO;2](https://doi.org/10.1175/1520-0442(1992)005%3c0541:AIOMFF%3e2.0.CO;2)
- Bunge L, Ochoa J, Badan A, Candela J, Sheinbaum J (2002) Deep flows in the Yucatan Channel and their relation to changes in the Loop Current extension. *J Geophys Res* 107(C12):3233. <https://doi.org/10.1029/2001JC001256>
- Candela J, Tanahara S, Crepon M, Barnier B, Sheinbaum J (2003) Yucatan Channel flow: observations versus CLIPPER ATL6 and MERCATOR PAM models. *J Geophys Res* 108(C12):3385. <https://doi.org/10.1029/2003JC001961>
- Candela J, Ochoa J, Sheinbaum J, Lopez M, Perez-Brunius P, Tenreiro M, Pallàs-Sanz E, Athié G, Arriaza-Oliveros L (2019) The flow through the Gulf of Mexico. *J Phys Oceanogr* 49(6):1381–1401. <https://doi.org/10.1175/JPO-D-18-0189.1>
- Chang Y-L, Oey L-Y (2012) Why does the Loop Current tend to shed more eddies in summer and winter? *Geophys Res Lett* 39:L05605. <https://doi.org/10.1029/2011GL050773>
- Chen Q, Wang L, Tawes R (2008) Hydrodynamic response of north-eastern Gulf of Mexico to hurricanes. *Estuaries Coasts* 31:1098–1116. <https://doi.org/10.1007/s12237-008-9089-9>
- Church JA, White NJ (2011) Sea-level rise from the late 19<sup>th</sup> to the early 21<sup>st</sup> century. *Surv Geophys* 32:585–602. <https://doi.org/10.1007/s10712-011-9119-1>
- Dangendorf S, Marcos M, Wöppelmann G, Conrad CP, Frederikse T, Riva R (2017) Reassessment of 20th century global mean sea level rise. *Proc Nat Acad Sci* 114(23):5946–5951. <https://doi.org/10.1073/pnas.1616007114>
- Dangendorf S, Hay C, Calafat FM, Marcos M, Piecuch CG, Berk K, Jensen J (2019) Persistent acceleration in global sea-level rise since the 1960s. *Nat Clim Change* 9:705–710. <https://doi.org/10.1038/s41558-019-0531-8>
- Dangendorf S, Frederikse T, Chafik L, Klinck J, Ezer T, Hamlington B (2021) Data-driven reconstruction reveals large-scale ocean circulation control on coastal sea level. *Nat Clim Change*. <https://doi.org/10.1038/s41558-021-01046-1>
- Ducet N, Le Tron PY, Reverdin R (2000) Global high-resolution mapping of ocean circulation from TOPEX/Poseidon and ERS-1&2. *J Geophys Res* 105:19,477–19,498. <https://doi.org/10.1029/2000JC900063>
- Elliott BA (1982) Anti-cyclonic rings in the Gulf of Mexico. *J Phys Oceanogr* 12:1292–1309. [https://doi.org/10.1175/1520-0485\(1982\)012%3c1292:ARITGO%3e2.0.CO;2](https://doi.org/10.1175/1520-0485(1982)012%3c1292:ARITGO%3e2.0.CO;2)
- Ezer T (2015) Detecting changes in the transport of the Gulf Stream and the Atlantic overturning circulation from coastal sea level data: the extreme decline in 2009–2010 and estimated variations for 1935–2012. *Glob Planet Change* 129:23–36. <https://doi.org/10.1016/j.gloplacha.2015.03.002>
- Ezer T, Corlett WB (2012) Is sea level rise accelerating in the Chesapeake Bay? A demonstration of a novel new approach for analyzing sea level data. *Geophys Res Lett* 39(19):L19605. <https://doi.org/10.1029/2012GL053435>
- Ezer T, Dangendorf S (2020) Global sea level reconstruction for 1900–2015 reveals regional variability in ocean dynamics and an unprecedented long weakening in the Gulf Stream flow since the 1990s. *Ocean Sci* 16(4):997–1016. <https://doi.org/10.5194/os-2020-22>
- Ezer T, Dangendorf S (2021) Variability and upward trend in the kinetic energy of western boundary currents over the last century: impacts from barostatic and dynamic sea level change. *Clim Dyn*. <https://doi.org/10.1007/s00382-021-05808-7>
- Ezer T, Dangendorf S (2022) Spatiotemporal variability of the ocean since 1900: testing a new analysis approach using global sea level reconstruction. *Ocean Dyn* 72:79–97. <https://doi.org/10.1007/s10236-021-01494-5>
- Ezer T, Mellor GL, Greatbatch RJ (1995) On the interpentadal variability of the North Atlantic ocean: model simulated changes

- in transport, meridional heat flux and coastal sea level between 1955–1959 and 1970–1974. *J Geophys Res* 100(C6):10,559–10,566. <https://doi.org/10.1029/95JC00659>
- Ezer T, Oey L-Y, Lee H-C, Sturges W (2003) The variability of currents in the Yucatan Channel: analysis of results from a numerical ocean model. *J Geophys Res* 108(C1):3012. <https://doi.org/10.1029/2002JC001509>
- Ezer T, Atkinson LP, Corlett WB, Blanco JL (2013) Gulf Stream's induced sea level rise and variability along the U.S. mid-Atlantic coast. *J Geophys Res* 118:685–697. <https://doi.org/10.1002/jgrc.20091>
- Forristal GZ, Schaudt KJ, Cooper CK (1992) Evolution and kinematics of a Loop Current eddy in the Gulf of Mexico during 1985. *J Geophys Res* 97:2173–2184. <https://doi.org/10.1029/91JC02905>
- Frederikse T, Landerer F, Caron L, Adhikari S, Parkes D, Humphrey VV, Dangendorf S, Hogarth P, Zanna L, Cheng L, Wu Y-H (2020) The causes of sea-level rise since 1900. *Nature* 584:393–397. <https://doi.org/10.1038/s41586-020-2591-3>
- Gehrels WR, Dangendorf S, Barlow NLM, Saher MH, Long AJ, Woodworth PL, Piecuch CG, Berk K (2020) A preindustrial sea-level rise hotspot along the Atlantic coast of North America. *Geophys Res Lett* 47. <https://doi.org/10.1029/2019GL085814>
- Goddard PB, Yin J, Griffies SM, Zhang S (2015) An extreme event of sea-level rise along the Northeast coast of North America in 2009–2010. *Nat Commun*. <https://doi.org/10.1038/ncomms7346>
- Greatbatch RJ, Fanning AF, Goulding AD, Levitus S (1991) A diagnosis of interpentadal circulation changes in the North Atlantic. *J Geophys Res Oceans* 96(C12):22009–22023. <https://doi.org/10.1029/91JC02423>
- Hall CA, Leben RR (2016) Observational evidence of seasonality in the timing of Loop Current eddy separation. *Dyn Atmos Ocean* 76(2):240–267. <https://doi.org/10.1016/j.dynatmoce.2016.06.002>
- Hamilton P (1992) Lower continental slope cyclonic eddies in the central Gulf of Mexico. *J Geophys Res* 97:2185–2200. <https://doi.org/10.1029/91JC01496>
- Hamilton P, Berger TJ, Johnson W (2002) On the structure and motions of cyclones in the northern Gulf of Mexico. *J Geophys Res* 107(C12):1–18. <https://doi.org/10.1029/1999JC000270>
- Hsueh Y, Marmorino GO, Vansant LL (1982) Numerical model studies of the winter-storm response of the West Florida shelf. *J Phys Oceanogr* 12:1037–1050. [https://doi.org/10.1175/1520-0485\(1982\)012%3c1037:NMSOTW%3e2.0.CO;2](https://doi.org/10.1175/1520-0485(1982)012%3c1037:NMSOTW%3e2.0.CO;2)
- Huang NE, Shen Z, Long SR, Wu MC, Shih EH, Zheng Q, Tung CC, Liu HH (1998) The empirical mode decomposition and the Hilbert spectrum for nonstationary time series analysis. *Proc R Soc London Ser A* 45:903–995. <https://doi.org/10.1098/rspa.1998.0193>
- Hurlburt HE, Thompson JD (1980) A numerical study of Loop Current intrusions and eddy shedding. *J Phys Oceanogr* 10:1611–1651. [https://doi.org/10.1175/1520-0485\(1980\)010%3c1611:ANSOLC%3e2.0.CO;2](https://doi.org/10.1175/1520-0485(1980)010%3c1611:ANSOLC%3e2.0.CO;2)
- Hurrell JW (1995) Decadal trends in the North Atlantic Oscillation: regional temperatures and precipitation. *Science* 269:676–679
- Jevrejeva S, Moore JC, Grinsted A, Woodworth PL (2008) Recent global sea level acceleration started over 200 years ago? *Geophys Res Lett* 35:L08715. <https://doi.org/10.1029/2008GL033611>
- Kenigson JS, Han W (2014) Detecting and understanding the accelerated sea level rise along the east coast of the United States during recent decades. *J Geophys Res Oceans* 119(12):8749–8766. <https://doi.org/10.1002/2014JC010305>
- Kourafalou VH, Androulidakis Y, Le Hénaff M, Kang H (2017) The dynamics of Cuba Anticyclones (CubANs) and interaction with the Loop Current/Florida Current System. *J Geophys Res Oceans* 122:7897–7923. <https://doi.org/10.1002/2017JC012928>
- Levitus S (1989) Interpentadal variability of temperature and salinity at intermediate depths of the North Atlantic Ocean, 1970–1974 versus 1955–1959. *J Geophys Res Oceans* 94(C5):6091–6131. <https://doi.org/10.1029/JC094iC05p06091>
- Lin Y, Greatbatch RJ, Jinyu Sheng J (2010) The influence of Gulf of Mexico Loop Current intrusion on the transport of the Florida Current. *Ocean Dyn* 60:1075–1084. <https://doi.org/10.1007/s10236-010-0308-0>
- Little CM, Hu A, Hughes CW, McCarthy GD, Piecuch CG, Ponte RM, Thomas MD (2019) The relationship between U.S. East Coast sea level and the Atlantic meridional overturning circulation: a review. *J Geophys Res* 124:6435–6458. <https://doi.org/10.1029/2019JC015152>
- Martínez-Moreno J, Hogg AM, England MH, Constantinou NC, Kiss AE, Morrison AK (2021) Global changes in oceanic mesoscale currents over the satellite altimetry record. *Nat Clim Change* 11:397–403. <https://doi.org/10.1038/s41558-021-01006-9>
- Maul GA (1977) The annual cycle of the Gulf Loop Current. Part I: observations during a one-year time series. *J Mar Res* 35:29–47
- Maul GA, Mayer DA, Baig SR (1985) Comparisons between a continuous 3-year current-meter observation at the sill of the Yucatan Strait, satellite measurements of Gulf Loop Current area, and regional sea level. *J Geophys Res* 90:9089–9096
- McCloskey TA, Bianchette TA, Liu K-B (2013) Track patterns of landfalling and coastal tropical cyclones in the Atlantic basin, their relationship with the North Atlantic Oscillation (NAO), and the potential effect of global warming. *Amer J of Clim Change* 2(3A):37300. <https://doi.org/10.4236/ajcc.2013.23A002>
- Meinen CS, Baringer MO, Garcia RF (2010) Florida Current transport variability: an analysis of annual and longer-period signals. *Deep-Sea Res* 57(7):835–846. <https://doi.org/10.1016/j.dsr.2010.04.001>
- Merrifield MA, Merrifield ST, Mitchum GT (2009) An anomalous recent acceleration of global sea level rise. *J Clim* 22:5772–5781. <https://doi.org/10.1175/2009JCLI2985.1>
- Molinari RL, Festa JF, Behringer DW (1978) The circulation in the Gulf of Mexico derived from estimated dynamic height fields. *J Phys Oceanogr* 8(6):987–996. [https://doi.org/10.1175/1520-0485\(1978\)008%3c0987:TCITGO%3e2.0.CO;2](https://doi.org/10.1175/1520-0485(1978)008%3c0987:TCITGO%3e2.0.CO;2)
- Nickerson AK, Weisberg RH, Liu Y (2022) On the evolution of the Gulf of Mexico Loop Current through its penetrative, ring shedding and retracted states. *Adv Space Res*. <https://doi.org/10.1016/j.asr.2022.03.039>
- Oey L-Y, Lee H-C, Schmitz WJ Jr (2003) Effects of winds and Caribbean eddies on the frequency of loop current eddy shedding: a numerical model study. *J Geophys Res* 108(C10):3324. <https://doi.org/10.1029/2002JC001698>
- Oey L-Y, Ezer T, Sturges W (2004) Modeled and observed empirical orthogonal functions of currents in the Yucatan Channel. *J Geophys Res* 109:C08011. <https://doi.org/10.1029/2004JC002345>
- Oey L-Y, Ezer T, Wang D-P, Fan S-J, Yin X-Q (2006) Loop Current warming by Hurricane Wilma. *Geophys Res Lett* 33:L08613. <https://doi.org/10.1029/2006GL025873>
- Park J, Sweet W (2015) Accelerated sea level rise and Florida current transport. *Ocean Sci* 11:607–615. <https://doi.org/10.5194/os-11-607-2015>
- Sallenger AH, Doran KS, Howd P (2012) Hotspot of accelerated sea-level rise on the Atlantic coast of North America. *Nature Clim Chan* 2:884–888. <https://doi.org/10.1038/NCILMATE1597>
- Sturges W, Evans JC (1983) Variability of Loop Current in Gulf of Mexico. *J Mar Res* 41:639–653. <https://doi.org/10.1357/002224083788520487>
- Sturges W, Leben R (2000) Frequency of ring separations from the Loop Current in the Gulf of Mexico: a revised estimate. *J Phys Oceanogr* 30:1814–1818. [https://doi.org/10.1175/1520-0485\(2000\)030%3c1814:FORSFT%3e2.0.CO;2](https://doi.org/10.1175/1520-0485(2000)030%3c1814:FORSFT%3e2.0.CO;2)
- Taylor AH, Stephens JA (1998) The North Atlantic Oscillation and the latitude of the Gulf Stream. *Tellus A* 50(1):134–142. <https://doi.org/10.3402/tellusa.v50i1.14517>
- Thiebaut HJ, Zwiers FW (1984) The interpretation and estimation of effective sample size. *J Clim Appl Meteorol* 23:800–811

- Tsimplis MN, Calafat FM, Marcos M, Jordá G, Gomis D, Fenoglio-Marc L, Struglia MV, Josey SA, Chambers DP (2013) The effect of the NAO on sea-level and on mass changes in the Mediterranean Sea. *J Geophys Res* 118:944–952. <https://doi.org/10.1002/jgrc.20078>
- Vukovich FM, Crissman BW, Bushnell M, King WJ (1979) Some aspects of the oceanography of the Gulf of Mexico using satellite and in situ data. *J Geophys Res* 84:7749–7768. <https://doi.org/10.1029/JC084iC12p07749>
- Wu Z, Huang NE (2009) Ensemble empirical mode decomposition: a noise-assisted data analysis method. *Adv Adapt Data Anal* 1(1):1–41. <https://doi.org/10.1142/S1793536909000047>
- Xu FH, Oey LY, Miyazawa Y, Hamilton P (2013) Hindcasts and forecasts of Loop Current and eddies in the Gulf of Mexico using local ensemble transform Kalman Filter and optimum-interpolation assimilation schemes. *Ocean Mod* 69:22–38. <https://doi.org/10.1016/j.ocemod.2013.05.002>
- Yin J, Goddard PB (2013) Oceanic control of sea level rise patterns along the East Coast of the United States. *Geophys Res Lett* 40:5514–5520. <https://doi.org/10.1002/2013GL057992>
- Hamilton P, Donohue K, Hall C, Leben RR, Quian H, Sheinbaum J, Watts DR (2014) Observations and dynamics of the Loop Current. US Dept. of the Interior, Bureau of Ocean Energy Management, New Orleans, LA, BOEM Report 2015–006, 417 pp.
- Hurrell JW, Kushnir Y, Ottersen G, Visbeck M (eds) (2003) The North Atlantic Oscillation: climate significance and environmental impact. *Geophys. Monogr. Ser.*, vol. 134. AGU, Washington, D. C
- Kantha L, Choi JK, Schaudt KJ, Cooper CK (2005) A regional data-assimilative model for operational use in the Gulf of Mexico. In: Sturges W, Lugo-Fernandez (eds) *Circulation in the Gulf of Mexico: Observations and Models*. *Amer Geophys Union Geophysical Monograph Ser.*, 161:165–180.
- Kolker AS, Allison MA, Hameed S (2011) An evaluation of subsidence rates and sea-level variability in the northern Gulf of Mexico. *Geophys Res Lett* 38(21). <https://doi.org/10.1029/2011GL049458>
- Moreles E, Zavala-Hidalgo J, Martínez-López B, Ruiz-Angulo A (2021) Influence of stratification and Yucatan Current transport on the Loop Current Eddy shedding process. *J Geophys Res Oceans* 126(1). <https://doi.org/10.1029/2020JC016315>
- Oey L-Y (2004) Vorticity flux through the Yucatan Channel and Loop Current variability in the Gulf of Mexico. *J Geophys Res* 104(C10). <https://doi.org/10.1029/2004JC002400>
- Oey L-Y, Ezer T, Lee H-C (2005) Loop Current, rings and related circulation in the Gulf of Mexico: a review of numerical models and future challenges. In: *Circulation in the Gulf of Mexico: Observations and Models*, W. Sturges and A. Lugo-Fernandez (Eds.). *Geophys Monogr Ser Vol 161*, pp. 31–56, AGU, Washington, DC. <https://doi.org/10.1029/161GM04>
- Prasad TG, Hogan PJ (2007) Upper-ocean response to Hurricane Ivan in a 1/25° nested Gulf of Mexico HYCOM. *J Geophys Res* 112(C4). <https://doi.org/10.1029/2006JC003695>
- Reid RO (1972) A simple dynamic model of the Loop Current. Contributions on the physical oceanography of the Gulf of Mexico, Vol II, Capurro LRA, Reid JL (eds). Gulf Publishing Co 157–159.
- Sheinbaum J, Candela J, Badan A, Ochoa J (2002) Flow structure and transports in the Yucatan Channel. *Geophys Res Lett* 29(3). <https://doi.org/10.1029/2001GL013990>

Springer Nature or its licensor (e.g. a society or other partner) holds exclusive rights to this article under a publishing agreement with the author(s) or other rightsholder(s); author self-archiving of the accepted manuscript version of this article is solely governed by the terms of such publishing agreement and applicable law.